Ultramicroscopy 136 (2014) 185–192

Contents lists available at ScienceDirect

Ultramicroscopy

journal homepage: www.elsevier.com/locate/ultramic

3D analysis of advanced nano-devices using electron and atom probe tomography

A. Grenier [a,*], S. Duguay [b], J.P. Barnes [a], R. Serra [a], G. Haberfehlner [a], D. Cooper [a], F. Bertin [a], S. Barraud [a], G. Audoit [a], L. Arnoldi [b], E. Cadel [b], A. Chabli [a], F. Vurpillot [b]

[a] CEA, LETI, MINATEC Campus, 17 rue des Martyrs, 38054 Grenoble Cedex 9, France
[b] Groupe de Physique des Matériaux, UMR 6634 CNRS—Université de Rouen, BP 12, 76801 Saint Etienne du Rouvray Cedex, France

ARTICLE INFO

Article history:
Received 25 June 2013
Received in revised form
17 September 2013
Accepted 8 October 2013
Available online 17 October 2013

Keywords:
Atom probe tomography
Tip shape simulation
Electron tomography
Quantification
Gate-all-around transistor
Tri-gate transistor

ABSTRACT

The structural and chemical properties of advanced nano-devices with a three-dimensional (3D) architecture have been studied at the nanometre scale. An original method has been used to characterize gate-all-around and tri-gate silicon nanowire transistor by combining electron tomography and atom probe tomography (APT). Results show that electron tomography is a well suited method to determine the morphological structure and the dimension variations of devices provided that the atomic number contrast is sufficient but without an absolute chemical identification. APT can map the 3D chemical distribution of the atoms in devices but suffers from strong distortions in the dimensions of the reconstructed volume. These may be corrected using a simple method based on atomic density correction and electron tomography data. Moreover, this combination is particularly useful in helping to understand the evaporation mechanisms and improve APT reconstructions. This paper demonstrated that a full 3D characterization of nano-devices requires the combination of both tomography techniques.
© 2013 Elsevier B.V. All rights reserved.

1. Introduction

The continuous down-scaling of semiconductor devices requires the development and integration of new materials into the complementary metal-oxide-semiconductor (CMOS) design. These approaches include the implementation of a high-k metal gate stack to overcome tunnelling leakage currents which occur in conventional gate oxides [1,2]. Gate-all-around Si nanowire transistors (GAA) and tri-gate Si nanowire transistors (tri-gate), which involve a deposition of the gate stack directly onto etched semiconductor Si nanowires are seen as promising candidates for CMOS technologies [3]. Their three dimensional nature offers a better gate control capability than planar structures and hence, they present immunity from leakage. The performances of planar-type devices are dependent on the doping distribution, the roughness and abruptness of interfaces [4]. These effects are dramatically enhanced in the case of 3D devices architecture [5]. Hence, in the case of FinFET structures, a targeted resistance state implies the achievement of a specific activated doping level on the sidewalls as it has been already reported [6,7]. This means that the electrical properties of such structures depend mainly on the doping distribution. Also, previous studies on GAA have demonstrated the benefits on the electrical characteristics of the hydrogen annealing used to round the sharp corners of the wires and to decrease their surface roughness [8]. The effective industrial development of these 3D devices requires the control of dimensions and compositions using characterization techniques with atomic scale capabilities. Thus the development of such techniques is an important challenge for the semiconductor industry.

Electron tomography is a transmission electron microscopy based technique that can be used to retrieve information in 3D [9,10] with a large probed volume up to $300 \times 300 \times 300\ \text{nm}^3$ from a series of 2-D projections at different tilt angles followed by 3D data processing. Scanning transmission electron microscopy (STEM) using a high angular annular dark field (HAADF) detector is well suited to perform tomography of semiconducting samples as diffraction effects are minimised. For electron tomography, the spatial resolution is anisotropic and varies from 2 nm to 5 nm depending on the tilt range, the number of acquired images and the size of the analysed sample [11]. For samples measuring a few hundreds of nanometres the resolution is in the nanometre range but for very small samples, electron tomography has shown to provide atomic resolution in combination with prior assumptions on the crystallographic orientations of the object [12,13]. Electron tomography has already been used to characterize GAA devices to demonstrate the hydrogen annealing effect on the square cross section of nanowires and the smoothing of their corners [14]. In addition to morphological information, STEM tomography can allow to distinguish the different elements, as it is sensitive to

* Corresponding author. Tel.: +33 4 38 08 45; fax: +33 4 38 78 52 73.
E-mail address: adeline.grenier@cea.fr (A. Grenier).

0304-3991/$ - see front matter © 2013 Elsevier B.V. All rights reserved.
http://dx.doi.org/10.1016/j.ultramic.2013.10.001

atomic number contrast (Z-contrast). However, if the difference between two atomic numbers is low, it can be difficult to map clearly the different elements. TEM techniques based on inelastic scattering of electrons have been successfully used for electron tomography for cases where HAADF STEM failed due to low Z-contrast. Among these techniques energy-filtered TEM (EFTEM) is most frequently used. EFTEM can be done in the core-loss range, where different elements can be identified by their ionization edges or in the low-loss range, where plasmon peaks can be used to distinguish between different materials [15–17]. Energy-electron loss spectroscopy (EELS) and energy-dispersive x-ray spectroscopy (EDS) are other TEM techniques based on inelastic scattering, which have also been combined with tomography. In principle these techniques could also allow chemical quantification, but their sensitivity is generally too low for most applications.

Atom probe tomography (APT) is based on atom by atom field evaporation from a sharply pointed sample, and it is expected to be one of the tools of choice for the analysis of current and future devices in terms of morphology and composition in three dimensions [18]. It can be considered as a quantitative 3D chemical high resolution microscope, with a field of view (FOV) up to 150 nm, that allows the spatial distribution of elements in a sample to be mapped in 3D at the atomic scale [19,20]. The recent development of APT with laser assisted evaporation [21,22] has made the analysis of semiconductor materials possible [23,24], giving access to the direct mapping of doping distribution (boron, arsenic, phosphorous etc.) as has been shown in MOSFET structures [25]. Recently, doping distribution determined by APT has been directly linked to electrical performances of FinFET devices [26]. Nevertheless, reconstruction artefacts, due to the presence of materials with different evaporation fields within a 3D structure, are shown to result in a strong deviation from the original structure [24]. The reconstructed shapes are often distorted (e.g. interfaces between different materials etc.) and the measured local compositions may be incorrect due to ion trajectory overlaps [27,28].

In the present work, we demonstrate that a full three dimensional morphological and chemical characterization of GAA and tri-gate devices that have been processed on SOI (Silicon on Insulator) substrates requires the combination of STEM tomography followed by APT tomography. In addition, the comparison between electron tomography and APT data highlights the distortion of the reconstructed APT volume. Results of the evaporation simulation of the GAA and tri-gate devices are analysed in order to understand the APT reconstructed volumes.

2. Material and methods

For this study, we used both GAA and tri-gate devices to evaluate the 3D characterization capabilities of electron tomography and APT. These devices are based on Si nanowires obtained from a (100) SOI substrate after anisotropic (for GAA) and isotropic (for tri-gate) etchings of the top Si layer on a 145 nm buried oxide (BOX). The Si nanowire is surrounded by a high-k metal gate stack. The nominal gate stack for the GAA device consists of 1 nm of SiO_2 (interlayer: IL), 3 nm of HfO_2 (high-k), 10 nm of TiN and 60 nm of poly-silicon, as shown in Fig. 1(a). The tri-gate gate stack shown in Fig. 1(b) is slightly different with a 0.8 nm interlayer, 1.7 nm HfSiON (high-k), 5 nm TiN and 50 nm of poly-silicon. The result is a 3-D gate stack around fifty Si nanowire channels with a length ranging from 20 nm to 1 μm. The GAA silicon nanowire transistor shows a square cross section with a width of 20 nm. The tri-gate transistor presents a height of 15 nm.

Electron tomography and APT investigations require a needle-shaped specimen preparation to avoid shadowing effects during tilt acquisition [29] and to promote field evaporation at the apex of the tip, respectively. These needles were specifically prepared with a Ga focused ion beam (FIB), using a 2 keV low energy beam during the final annular milling, which reduces irradiation damages on the sidewalls of the tip. We have used two different mountings of the sample for the electron tomography (omniprobe® grid) and APT (a picoprobe® tip) experiments. This means that different samples made from the 3D structure have been investigated by each of the two tomography techniques.

Electron tomography experiments were carried out using a probe-corrected Titan from FEI in the HAADF STEM imaging mode with the microscope operated at 200 keV. A convergence angle of 5 mrad was chosen for the electron beam to increase the depth of focus up to 80 nm [30]. Series of 2D STEM images were acquired using a holder from Fischione and the 3-D reconstructions were then carried out using the Inspect 3D software from FEI.

For the GAA structure, the electron tomography acquisition was performed with a tilt range of $\pm 75^{\circ}$ and with increments of 1°. As the tilt range is limited, missing wedge artefacts may be induced in the reconstructed volume along the axis defined by the electron beam. To avoid it, two different configurations were prepared for the GAA structure. On the one hand the silicon nanowire is aligned perpendicular to the tip axis in the top-down geometry (Fig. 2(a)). The electron beam direction in the TEM at 0° tilt coincides with the direction of the nanowire. This configuration allows the nanowire section to be well-resolved, according to weighted backprojection (WBP) algorithm simulations using 151 slices. On the other hand the silicon nanowire channel axis is parallel to the tip axis in the cross-section geometry (Fig. 2(b)). This configuration allows the fluctuations of the nanowire dimensions to be measured along the nanowire axis. For both configurations, the 3-D reconstructions were obtained using simultaneous iterative reconstruction technique (SIRT) algorithm [31].

Concerning the tri-gate structure, a different approach based on the dual axis tomography has been employed using only the top-down geometry. Thus the missing wedge artefacts are limited and the resolution of the reconstructed volume is improved. For that, two tilt series have been acquired around two perpendicular tilt axes. The tilt range was $\pm 78^{\circ}$ around the first axis and approximately $\pm 50^{\circ}$ around the second one. For both axes a tilt step of 1° was used. The 3D reconstruction was obtained from an in-house dual-axis SIRT algorithm described elsewhere [32].

The APT investigations were performed using a LAWATAP from CAMECA with an amplified ytterbium doped laser at a wavelength of 343 nm with energy of 35 nJ/pulse providing a 350 fs pulse duration, a spot size of 300 μm and a 100 kHz repetition rate. Only the top-down geometry was used to increase the spatial resolution along the high-k metal gate stack. The APT data were reconstructed using standard procedures mainly based on the Gault et al. protocol [33].

3. Results and discussion

3.1. Electron tomography results

A 3D isosurface representation of the GAA structure is shown in Fig. 3(a) together with an orthoslice in Fig. 3(c) through the 3D reconstructed volume. These are shown using a top-down and a cross-section geometry, respectively. The threshold for the isosurface rendering has been set at the intensity level of the TiN encapsulating layer. In this case, the Si nanowire channel is not directly represented, but the location of its boundary is inferred from the shape of the surrounding high-k layer. On the slice from the cross-section GAA tomogram, the Z-contrast is enough to discriminate TiN and HfO_2 (bright contrast). However, the interface between the silicon oxide interlayer and the Si channel is not

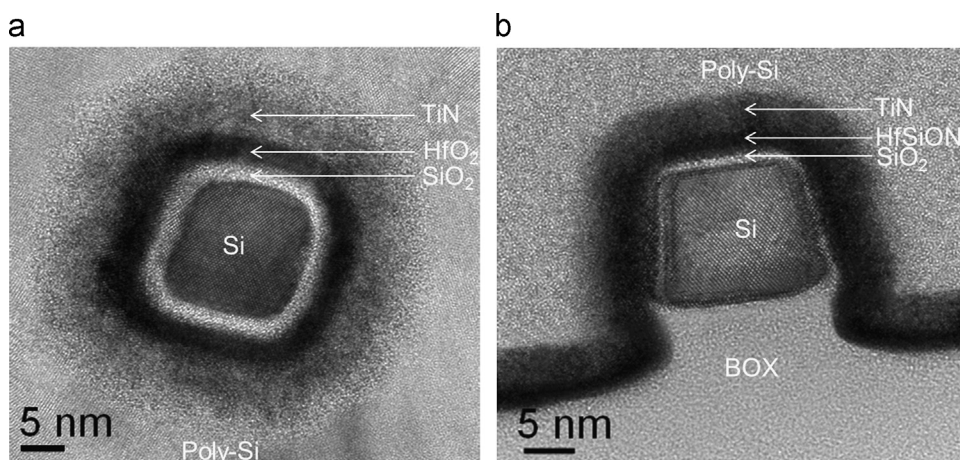

Fig. 1. Cross-sectional TEM images of GAA (a) and tri-gate (b) transistors.

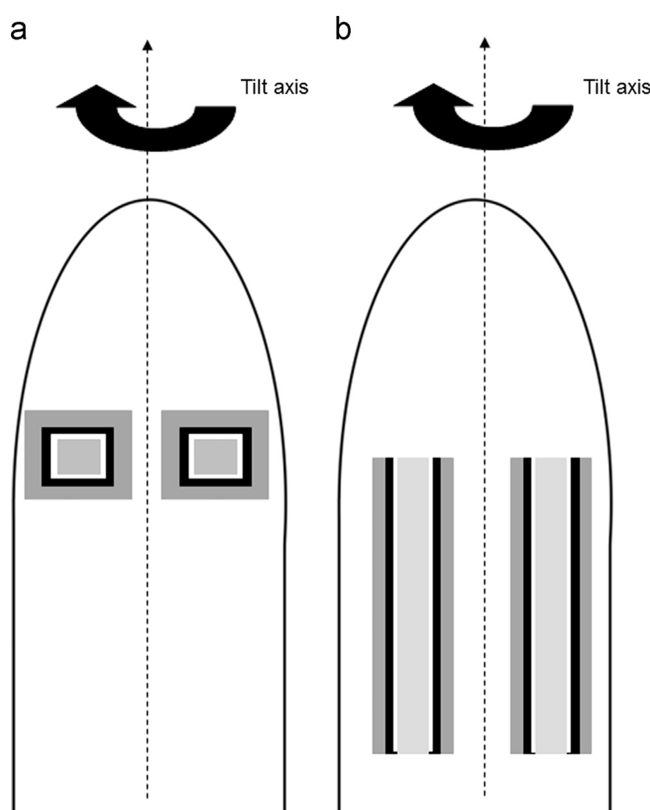

Fig. 2. Scheme of the top-down (a) and cross-section (b) geometries used for tomography experiments.

clearly detected as the average Z-numbers of these materials are close. But, the variations of the combined silicon and silicon oxide interlayer have been assessed along the Si nanowire on 20 slices leading to the measurement of an average radius of 17.2 ± 0.8 nm. Also, from this reconstruction, a mean value of the high-k layer has been estimated to 2.4 ± 0.2 nm, lower than the nominal thickness (3 nm).

For the tri-gate structure, a segmentation showing the metal gate and the high-k dielectric is presented in the Fig. 3(b). A slice along the nanowire axis through the reconstructed volume is shown in Fig. 3(d). As for the GAA device, it is delicate to determine the interface between the silicon oxide interlayer and the silicon channel. However, based on this reconstruction, information about geometrical parameters could be measured such as the width of the nanowire channel which varies from 20 nm at the top of the nanowire to 26 nm at the bottom. From this reconstruction the mean value of the local high-k layer thickness of 1.65 ± 0.25 nm could also be measured. Though this value is close to the nominal one, its accuracy may be limited by several factors, such as alignment of the tilt series, spot size of the electron beam and the voxel size of $0.26 \times 0.26 \times 0.26$ nm^3.

In summary, STEM HAADF tomography allows the morphology and dimensions of devices to be characterized with a large FOV. However it suffers from two main limitations: (i) insufficient Z-contrast for distinguishing the silicon oxide interlayer from the Si channel, (ii) no composition quantification.

3.2. Atom probe tomography results

Fig. 4(a) and (b) presents a 3D APT element map (each dot represents one atom) of a single GAA and tri-gate, respectively, using a basic shank angle reconstruction algorithm [34]. The top-down geometry has been used to increase the depth resolution. All chemical species are identified by the time-of-flight measurement leading to a mass spectrum of atoms and/or molecules within the analysed volume. The different position of the devices in the analysed tip is due to the fact that one face of the nanowire is directly in contact with the SiO_2 layer of the SOI substrate for the tri-gate structure, whereas the remaining faces are surrounded by the transistor dielectrics (SiO_2, HfO_2) for the GAA structure. The high-k contribution HfO during analysis of these devices is found to be different from the nominal one. In addition to the intrinsic spatial resolution of APT, the silicon oxide interlayer can be easily discriminated from the Si channel.

The reconstructed volumes show strong deviations from the morphology observed by electron tomography. It should be noted that the chemical identification is not affected by these artefacts.

Both of the devices have a deformed shape. A lateral compression of the Si core of the device is observed rather than the expected square and side shapes. This strong compression of the Si nanowire channel observed after APT reconstruction leads to incorrect dimensions and shape if measured from the reconstructed volume. Addition deformations ("S-shape") that seem to be related to distance of the feature to the tip axis are observed. These distortions are due to the well-known local magnification effect in the context of a very complicated structure in term of evaporation fields, shapes and positions of the phases. It is explained by the fact that the evaporation field of the Si atoms of the nanowire is lower than that of the surrounding materials. Thus, the ion trajectories are focused, which induces a local enhancement of the measured atomic density and a compression

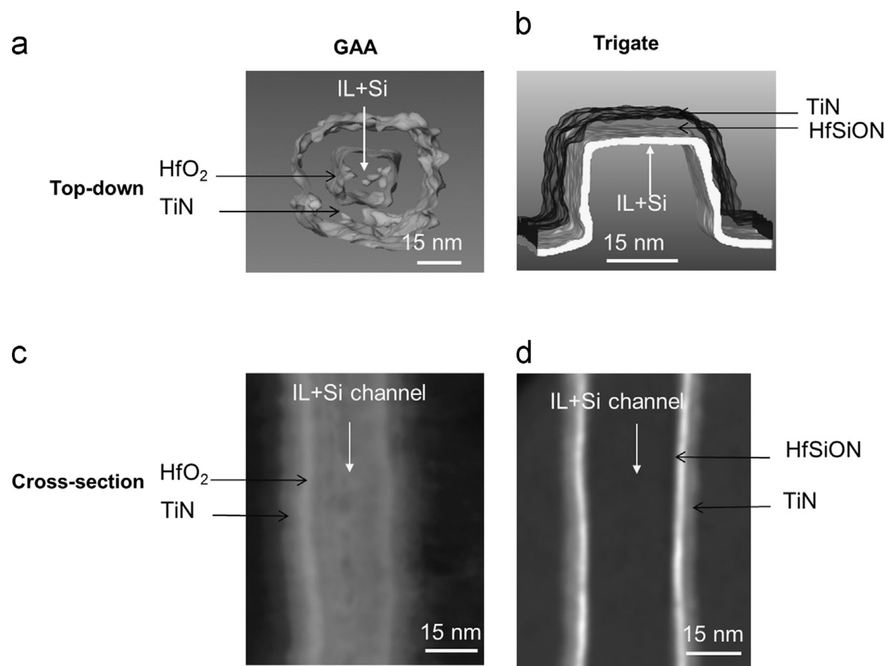

Fig. 3. Isosurface rendering (a) and (b) with orthogonal slices through the reconstructed volume (c) and (d) for GAA and tri-gate silicon nanowire transistor, respectively. IL is the silicon oxide interlayer for both structures.

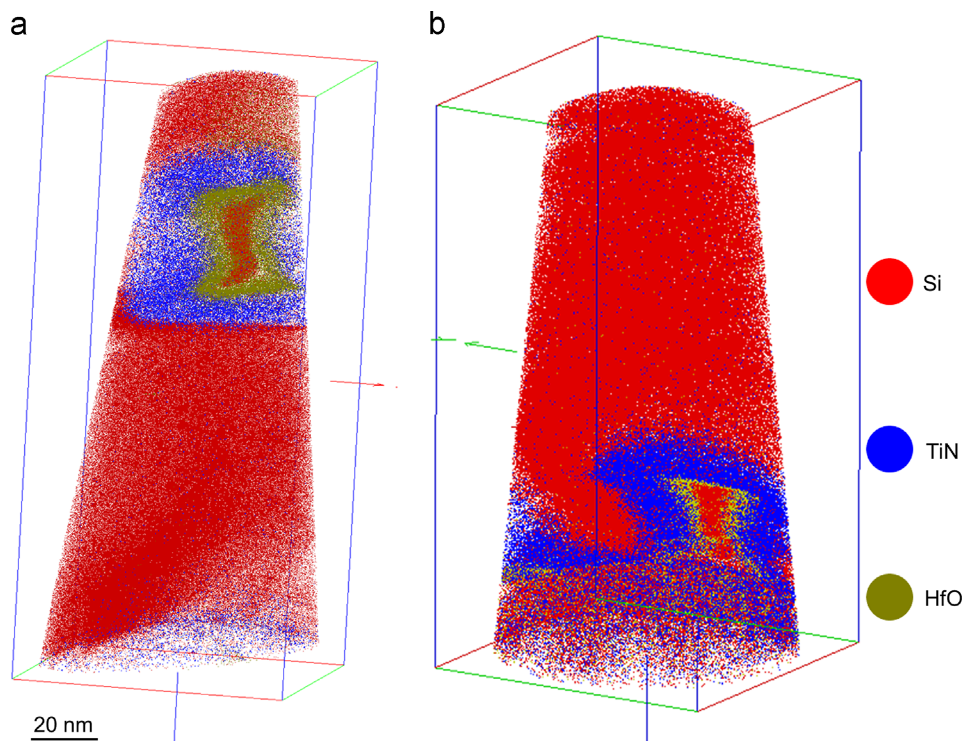

Fig. 4. 3D APT volume based on standard reconstruction algorithm for GAA (a) and tri-gate (b) silicon nanowire transistor. The chemical identification is deduced from mass over charge ratio.

of the lateral dimension of the core of the nanowire. This artefact leads to an over estimate of the densities of the Si nanowire and hence to incorrect dimensions.

3.3. Atom probe tomography simulation results

To understand the origin of the distortions in the APT reconstructed volumes compared to the electron tomography ones, simulations of the evaporation of the atoms in such structures have been performed. They are based on a 3D numerical code and take into account the different evaporation fields in each layer. The evaporation field F_{ev} is the critical field required to ensure the standing erosion of the sample. It depends on the voltage V applied to the tip and the end-radius R of the tip through the following relation $F_{ev}=V/\beta R$, where β is a quasi-constant geometric factor during the analysis.

The field evaporation process is simulated as the removal of surface atoms, considered as metallic cells, under the influence of

a high surface electric field. This field is resulting from the application of a high voltage to the specimen composed of a compact stack of atomic cells confined in a tip shape. Each atom is then defined by an assembly of numerical potential points. Once an atom is field evaporated, the atomic cell is removed and an ion leaves the surface. The trajectories of the ions are used to determine the tip to detector image projection. The elemental nature of the phases modelled inside the specimen is taken into account by using the field evaporation constants of the different contributions in each layer. More details can be found in the literature [35–37]. To simulate the field evaporation, the amplitude of the electric field is measured above all surface atoms, with the atom subjected to the highest field chosen as the next atom to be removed from the surface. The selected unit cell is removed and the electrostatic potential is recalculated over the whole volume. With this model, the gradual evolution of the field, the impacts of the ions on the detector and the gradual evolution of the tip shape are all simulated.

This model requires knowledge of the values of the evaporation field which are tabulated for homogeneous bulk materials [38]. When analysing a phase composed of two different element, the tip develops two local radii at the tip surface, giving rise to variations in magnification [27,39,40]. The field evaporations of each material in the GAA device have been roughly estimated using the method of Jeske and Schmitz [41]. Thus, the voltage variation in GAA has been measured during the evaporation of three different interfaces Si/SiO_2, Si/TiN and Si/HfO_2 from three different samples analysed by APT. The voltage variations are mainly induced by the relative evaporation fields of the SiO_2, TiN and HfO_2 compared to the tabulated Si phase. The evaporation field of SiO_2 interlayer was estimated to be around 43 V/nm, which is about 25% higher than pure Si in agreement with previous estimations [42]. The evaporation fields of TiN (38 V/nm) and HfO_2 (51 V/nm) are also higher than Si by about 15% and 45%, respectively.

The tip shapes simulated using these evaporation fields are shown in Fig. 5(a–e) at different steps of the field evaporation process of the GAA structure. While the Si phase is evaporated as a quasi-flat surface far from the GAA structure, the low evaporation field of Si compared to the surrounding HfO_2 and SiO_2 oxides gives rise to a large difference in local radius above the Si nanowire. This is clearly observed on the enlarged region of Fig. 5(g) and (h). The surrounding oxide appears protruding at the tip surface as it is field evaporated. This high positive curvature increases significantly the magnification in the TiN/HfO_2/SiO_2 region. Conversely, the inside nanowire surface shows a flat or close to negative curvature that focuses the ion trajectories in silicon and distorts strongly the image projection. The 3D reconstruction resulting from the simulation of the field evaporation process is shown in Fig. 5(f) that corresponds to a slice across the channel axis of the GAA structure. The initial square shape is compressed for the simulated Si channels as it is observed in the APT experimental reconstruction.

These results demonstrate the direct impact of an environment with a higher evaporation field which is responsible for a trajectory compression. Hence the local magnification effect is confirmed. This distortion comes from the dynamic evolution of the tip shape during the field evaporation process [27]. Nevertheless, the experimental deformation is clearly more pronounced than the simulated ones. This implies that complementary parameters have to be added in the simulation of the evaporation of GAA silicon nanowire transistor to reproduce the artefacts that are experimentally observed. Previous works [36] have shown that the permittivity values of the material in the evaporation simulation affects the field evaporation behaviour of dielectric materials. Hence taking into account the permittivity values for the simulation of the GAA and tri-gate structures is very promising since the permittivity ratio between HfO_2 and SiO_2 is significant (close to 6). Very recently, a new model proposed by Vurpillot et al. [43] suggests that residual conductivity in bulk oxides and dielectrics has to be taken into account too as the permittivity parameters do not completely explain the observed experimental distortion.

3.4. Combination of electron and atom probe tomography results

To improve the APT reconstruction regarding TEM and STEM tomography investigations, a procedure described elsewhere [44] and based on the correction of the atomic density was used. The average dimension of the nanowire determined by electron tomography experiments has been used to find the best fitting parameters for the APT reconstructions after the first order density corrections. These corrections only affect the local atomic density, keeping unchanged the local composition in the image. The resulting reconstruction, using standard shank angle algorithm, is shown in Fig. 6(a) and (b) for the GAA and tri-gate, respectively. Even if some important distortions remain, the shape and dimensions of the GAA transistor are now in good correlation with the dimensions measured by electron tomography.

The quantification of each layer within the gate stack of GAA and tri-gate is now possible. This means that determination of the dimension variations of the channel in 3D can be evaluated and included in simulations of electronic transport to estimate the impact of their roughness. Moreover, concentration profiles through the gate stack can also be extracted from these improved reconstructions as shown for the GAA in Fig. 7. Each data point is obtained from integrating the counts of the mass spectrum in a 0.1 nm thick sampling box within the white rectangular indicated on the APT reconstruction inset. The small size of the volume used to extract the profiles limits the number of the atoms involved in the concentration calculation and enhances the sensitivity to the local roughness of the interfaces. Thus the concentration profiles are intrinsically affected by errors that may be up to several per cent depending on the analysed element.

For TiN/HfO_2/SiO_2/Si structures, mass overlaps in the mass spectrum are highly pronounced. As an example, TiN evaporates mainly as Ti^{2+}, Ti^{3+}, TiN^{2+}, TiN^{+}, and N^{+}. Ti^{3+} overlaps with ${O_2}^{2+}$, N^{+} with Si^{2+}, Ti^{2+} with SiO^{2+}, TiN^{2+} with ${O_2}^{+}$ and even HfO^{3+} with TiN^{+}. This means that the reliable extraction of a quantitative concentration profile requires a fine analysis of the local mass spectrum in particular at the interfaces. In that case, when two elements overlap in mass, the concentration is estimated considering the isotopic ratio in the layers as far as possible from the interfaces.

The Si/SiO_2 and the HfO_2/TiN interfaces indicated by the dotted lines on Fig. 6 have been determined at the mid of the rising edge of the concentration variation curve. The SiO_2/HfO_2 interface has been placed on Fig. 7 regarding the oxygen concentration variation. Indeed, the SiO_2 layer corresponds to the region where the oxygen concentration is almost constant and its thickness is just below 1 nm. This leads to a thickness of 1.6 nm for the HfO_2 layer. Even if the deposited high-k layer is thinner than the nominal one as indicated by the electron tomography results, further improvement of the reconstructions should be reached to explain the discrepancy between APT and electron tomography thickness results. In addition, the concentration profile shown in Fig. 7 and also a localized mass spectrum (not shown here) in the high-k layer demonstrate the presence of Si atoms in this layer. Two processes may be responsible: (i) an effective intermixing of SiO_2 (or even Si from the substrate) and HfO_2 or (ii) an artificial mixing coming from local magnification effects described previously. Further investigations have to be conducted with the same chemical stack performed on 2D planar structures to analyse the specific evaporation parameters. In particular, APT analysis should

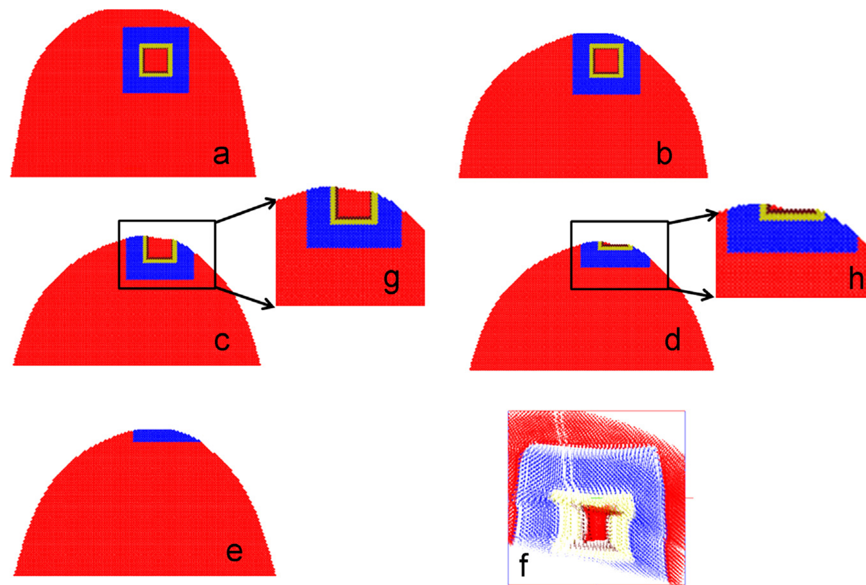

Fig. 5. Simulation of the field evaporation: (a–e) evolution of the tip profile induced by the field evaporation process. (f) Slice across the channel axis of the reconstructed GAA structure resulting from the field evaporation simulation. Tip shape deformations induce large distortions of the initial square shape of the GAA by focusing the ion trajectories. The Si channel appears contracted due to a lower evaporation field compared to the SiO_2/HfO_2 surrounding layers.

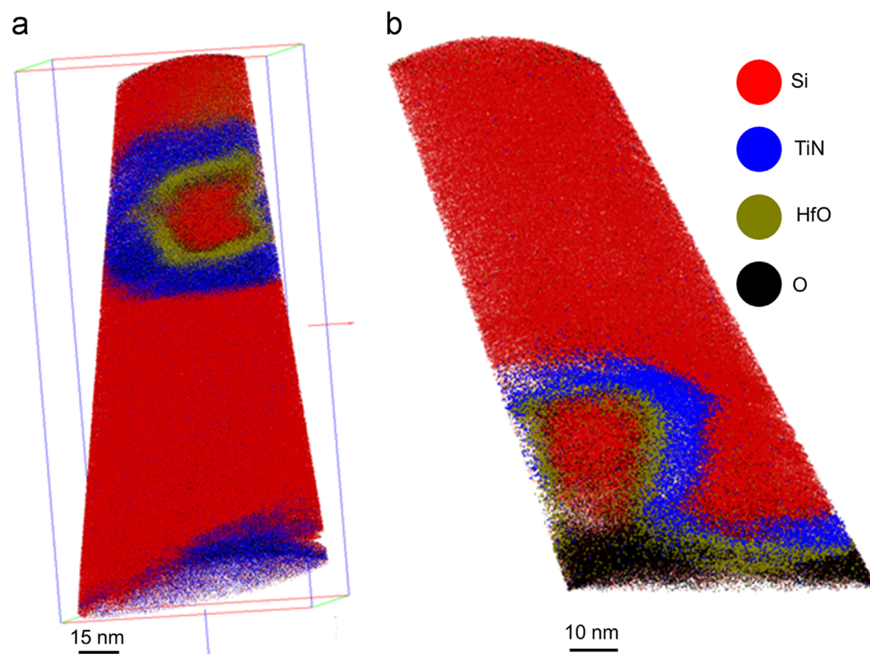

Fig. 6. 3D APT volume based on standard reconstruction algorithm after density correction of GAA (a) and tri-gate (b) silicon nanowire transistor.

be performed using both frontside and backside sample preparation to evaluate if preferential evaporation of different atoms occurs.

Despite these issues, it is clear that APT is uniquely placed to provide quantification of the elements present in such complicated structures in three-dimensions, extending what is possible by electron tomography alone.

4. Conclusion

This work shows the advantage of combining atom probe and electron tomography to analyse both morphology and composition of new device architectures such as GAA or tri-gate devices. The samples must be prepared in the shape of tips for both techniques. Electron tomography is a rapid way to determine the dimension variations when spatial resolution and atomic contrast are sufficient, but without an absolute chemical identification and quantification. Due to its spatial resolution combined with its mass sensitivity, APT demonstrated its capacity to separate each chemical contribution into layers with a sub-nanometre scale. However, the evolving tip shape during APT analysis determines the effective specifications of the microscope. Hence strong distortions are observed in APT reconstructions due to local magnification effects induced by differences in the evaporation fields of the materials. A simple method based on atomic density correction demonstrated the

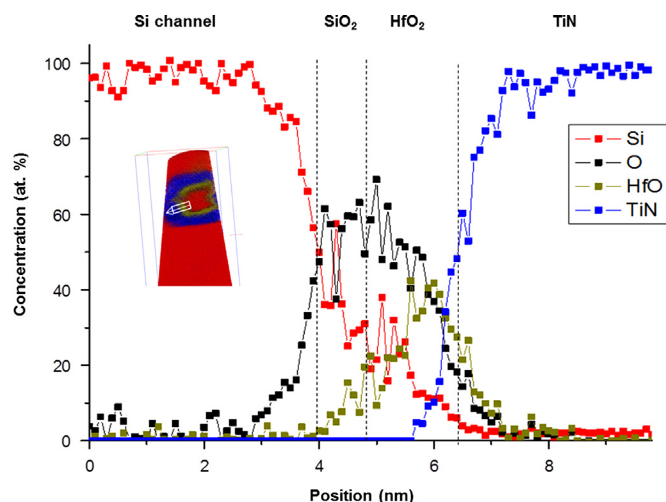

Fig. 7. Concentration profiles extracted after improved reconstructions from the centre of the Si channel (left) of the GAA device to the TiN gate (right). The white rectangular corresponds to the area where the concentration profile has been calculated.

possibility for better 3D reconstruction of devices. Better reconstruction procedures must be developed and will need better knowledge in the field evaporation behaviour under laser illumination of the chemical species involved in those devices. Performing electron tomography and APT on the same tip will be primordial to understand field evaporation and improve the reconstructions in order to obtain a full 3D characterisation of analysis of semiconductor devices.

Acknowledgements

This work has been financially supported by the Recherche Technologique de Base (RTB) and the French National Agency (Project no. APTITUDE ANR-12-NANO-0001). The experiments were performed on the Nanocharacterisation platform at MINATEC.

References

[1] G.D. Wilk, R.M. Wallace, J.M. Anthony, High-kappa gate dielectrics: current status and materials properties considerations, J. Appl. Phys. 89 (2001) 5243–5275.
[2] E.P. Gusev, V. Narayanan, M.M. Frank, Advanced high-k dielectric stacks with polySi and metal gates: recent progress and current challenges, IBM J. Res. Dev. 50 (2006) 387–410.
[3] P. Jong-Tae, J.P. Colinge, Multiple-gate SOI MOSFETs: device design guidelines, IEEE Trans. Electron. Devices 49 (2002) 2222–2229.
[4] S. Roy, A. Asenov, Where do the dopants go? Science 309 (2005) 388–390.
[5] W. Vandervorst, J.L. Everaert, E. Rosseel, M. Jurczak, T. Hoffman, P. Eyben, J. Mody, G. Zschatzsch, S. Koelling, M. Gilbert, T. Poon, J.d.A. Borniquel, M. Foad, R. Duffy, B.J. Pawlak, Conformal doping of FINFETs: a fabrication and metrology challenge, AIP Conf. Proc. 1066 (2008) 449–456.
[6] H. Takamizawa, Y. Shimizu, Y. Nozawa, T. Toyama, H. Morita, Y. Yabuuchi, M. Ogura, Y. Nagai, Dopant characterization in self-regulatory plasma doped fin field-effect transistors by atom probe tomography, Appl. Phys. Lett. 100 (2012) 093502–093503.
[7] N. Collaert, S. Brus, A. De Keersgieter, A. Dixit, I. Ferain, M. Goodwin, A. Kottantharayil, R. Rooyackers, P. Verheyen, Y. Yim, P. Zimmerman, S. Beckx, B. Degroote, M. Demand, M. Kim, E. Kunnen, S. Locorotondo, G. Mannaert, F. Neuilly, D. Shamiryan, C. Baerts, M. Ercken, D. Laidler, F. Leys, R. Loo, J. Lisoni, J. Snow, R. Vos, W. Boullart, I. Pollentier, S. De Gendt, K. De Meyer, M. Jurczak, S. Biesemans, Proceedings of the International Conference on Integrated Circuit and Technology, 2005, p. 187.
[8] E.T. Dornel E, J C Barbe, J-M Hartmann, V Delaye, F Aussenac, C Vizioz, S Borel, V Maffini-Alvaro, C, F.J Isheden, Appl. Phys. Lett. 91 (2007) 233502.
[9] E. Biermans, L. Molina, K.J. Batenburg, S. Bals, G. Van Tendeloo, Measuring porosity at the nanoscale by quantitative electron tomography, Nano Lett. 10 (2010) 5014–5019.
[10] I. Arslan, T.J.V. Yates, N.D. Browning, P.A. Midgley, Embedded nanostructures revealed in three dimensions, Science 309 (2005) 2195–2198.
[11] R.A. Crowther, D.J. Derosier, A. Klug, Reconstruction of 3 dimensional structure from projections and its application to electron microscopy, Proc. R. Soc. Lond. Ser. A—Math. Phys. Sci. 317 (1970) 319, http://dx.doi.org/10.1098/rspa.1970.0119.
[12] S. Van Aert, K.J. Batenburg, M.D. Rossell, R. Erni, G. Van Tendeloo, Three-dimensional atomic imaging of crystalline nanoparticles, Nature 470 (2011) 374–377.
[13] B. Goris, S. Bals, W. Van den Broek, E. Carbo-Argibay, S. Gomez-Grana, L.M. Liz-Marzan, G. Van Tendeloo, Atomic-scale determination of surface facets in gold nanorods, Nat. Mater. 11 (2012) 930–935.
[14] P.D. Cherns, F. Lorut, C. Dupré, T. Tachi, D. Cooper, A. Chabli, T. Ernst, Electron tomography of gate-all-around nanowire transistors, J. Phy.: Conf. Ser. 209 (2010) 012046.
[15] A. Yurtsever, M. Weyland, D.A. Muller, Three-dimensional imaging of non-spherical silicon nanoparticles embedded in silicon oxide by plasmon tomography, Appl. Phys. Lett. 89 (2006) 151920–151923.
[16] M.H. Gass, K.K.K. Koziol, A.H. Windle, P.A. Midgley, Four-dimensional spectral tomography of carbonaceous nanocomposites, Nano Lett. 6 (2006) 376–379.
[17] G. Haberfehlner, P. Bayle-Guillemaud, G. Audoit, D. Lafond, P.H. Morel, V. Jousseaume, T. Ernst, P. Bleuet, Four-dimensional spectral low-loss energy-filtered transmission electron tomography of silicon nanowire-based capacitors, Appl. Phys. Lett. 101 (2012) 063108.
[18] D.J. Larson, D. Lawrence, W. Lefebvre, D. Olson, T.J. Prosa, D.A. Reinhard, R.M. Ulfig, P.H. Clifton, J.H. Bunton, D. Lenz, J.D. Olson, L. Renaud, I. Martin, T.F. Kelly, Toward atom probe tomography of microelectronic devices, J. Phys.: Conf. Ser. 326 (2011) 012030.
[19] D. Blavette, A. Bostel, J.M. Sarrau, B. Deconihout, A. Menand, An atom probe for three-dimensional tomography, Nature 363 (1993) 432–435.
[20] D. Blavette, E. Cadel, A. Fraczkiewicz, A. Menand, Three-dimensional atomic-scale imaging of impurity segregation to line defects, Science 286 (1999) 2317–2319.
[21] G.L. Kellogg, T.T. Tsong, Pulsed-laser atom-probe field-ion microscopy, J. Appl. Phys. 51 (1980) 1184–1193.
[22] B. Gault, F. Vurpillot, A. Vella, M. Gilbert, A. Menand, D. Blavette, B. Deconihout, Design of a femtosecond laser assisted tomographic atom probe, Rev. Sci. Instrum. 77 (2006) 043705–043708.
[23] E. Cadel, F. Vurpillot, R. Lardé, S. Duguay, B. Deconihout, Depth resolution function of the laser assisted tomographic atom probe in the investigation of semiconductors, J. Appl. Phys. 106 (2009) 044908.
[24] M. Gilbert, W. Vandervorst, S. Koelling, A.K. Kambham, Atom probe analysis of a 3D finFET with high-k metal gate, Ultramicroscopy 111 (2011) 530–534.
[25] K. Inoue, F. Yano, A. Nishida, H. Takamizawa, T. Tsunomura, Y. Nagai, M. Hasegawa, Dopant distributions in n-MOSFET structure observed by atom probe tomography, Ultramicroscopy 109 (2009) 1479–1484.
[26] H. Takamizawa, Y. Shimizu, K. Inoue, T. Toyama, F. Yano, A. Nishida, T. Mogami, N. Okada, M. Kato, H. Uchida, K. Kitamoto, T. Miyagi, J. Kato, Y. Nagai, Correlation between threshold voltage and channel dopant concentration in negative-type metal-oxide-semiconductor field-effect transistors studied by atom probe tomography, App. Phy. Lett. 100 (2012) 253504.
[27] M.K. Miller, M.G. Hetherington, Local magnification effects in the atom probe, Surf. Sci. 246 (1991) 442–449.
[28] D. Blavette, P. Duval, L. Letellier, M. Guttmann, TEM Atomic-scale APFIM, investigation of grain boundary microchemistry in Astroloy nickel base superalloys, Acta Mater. 44 (1996) 4995–5005.
[29] P.D. Cherns, F. Lorut, S. Becu, C. Dupre, K. Tachi, D. Cooper, A. Chabli, T. Ernst, A study of gate-all-around transistors by electron tomography, in: D.G. Seiler, A.C. Diebold, R. McDonald, C.M. Garner, D. Herr, R.P. Khosla, E.M. Secula (Eds.), Frontiers of Characterization and Metrology for Nanoelectronics: 2009, American Institute of Physics, Melville, 2009, pp. 290–293.
[30] J. Biskupek, J. Leschner, P. Walther, U. Kaiser, Optimization of STEM tomography acquisition—a comparison of convergent beam and parallel beam STEM tomography, Ultramicroscopy 110 (2010) 1231–1237.
[31] P. Gilbert, Iterative methods for the three-dimensional reconstruction of an object from projections, J. Theor. Biol. 36 (1972) 105–117.
[32] G. Haberfehlner, R. Serra, D. Cooper, S. Barraud, P. Bleuet, 3D spatial resolution improvement by dual-axis electron tomography: application to tri-gate transistors, Ultramicroscopy 136 (2014) 144–153.
[33] B. Gault, M. Moody, J. Cairney, S. Ringer, Tomographic reconstruction, Springer, New York (2012) 2012; 169–171. (Atom Probe Microscopy).
[34] F. Vurpillot, M. Gruber, G. Da Costa, I. Martin, L. Renaud, A. Bostel, Pragmatic reconstruction methods in APT, Ultramicroscopy 111 (8) (2011) 1286–1294.
[35] Bostel Vurpillot, Blavette, The shape of field emitters and the ion trajectories in three-dimensional atom probes, J. Microsc. 196 (1999) 332–336.
[36] C. Oberdorfer, G. Schmitz, On the field evaporation behavior of dielectric materials in three-dimensional atom probe: a numeric simulation, Microsc. Microanal 17 (2011) 15–25.
[37] M. Gruber, F. Vurpillot, A. Bostel, B. Deconihout, Field evaporation: a kinetic Monte Carlo approach on the influence of temperature, Surf. Sci. 605 (2011) 2025–2031.
[38] T.T. Tsong, Field ion image formation, Surf. Sci. 70 (1978) 211–233.
[39] F. Vurpillot, A. Bostel, D. Blavette, A new approach to the interpretation of atom probe field-ion microscopy images, Ultramicroscopy 89 (2001) 137–144.
[40] D.G. Brandon, On field evaporation, Philos. Mag. 14 (1966) 803–820.

[41] T. Jeske, G. Schmitz, Influence of the microstructure on the interreaction of Al/Ni investigated by tomographic atom probe, Mater. Sci. Eng.: A 327 (2002) 101–108.
[42] E. Talbot, R. Lardé, F. Gourbilleau, C. Dufour, P. Pareige, Si nanoparticles in SiO_2: an atomic scale observation for optimization of optical devices, Europhys. Lett. 87 (2009) 26004.
[43] F. Vurpillot, A. Gaillard, G. Da Costa, B. Deconihout, A model to predict image formation in atom probetomography, Ultramicroscopy 132 (2013) 152–157.
[44] F. De Geuser, W. Lefebvre, F. Danoix, F. Vurpillot, B. Forbord, D. Blavette, An improved reconstruction procedure for the correction of local magnification effects in three-dimensional atom-probe, Surf. Interface Anal. 39 (2007) 268–272.